Fuel Flexibilization of a Small Scale Low-Swirl Burner for Biogas and Hydrogen

André Silva Justino
andre.justino@tecnico.ulisboa.pt

Instituto Superior Técnico - Universidade de Lisboa, Portugal

November 2020

Abstract

The current environmental concerns have led to increased restrictions on emissions and a higher demand of methods capable of achieving both lower pollutant emission levels and incorporating environmentally friendly fuels such as biogas. These should ideally be able to stabilize flames under leaner conditions, with the goal of lowering the NO_x emission levels. Development of swirled flames, a design based on adding rotation to the flow, has been ongoing for decades, and has eventuated the low-swirl burner (LSB) design. Although several studies have been made on the scalability and fuel flexibility of the design, most previous work has focused on higher thermal loads and larger burners. This study ponders the possibility of using a smaller burner and evaluates the stability limits for different compositions of biogas and hydrogen as fuel. Tests showed that hydrogen-enriched flames exhibited blow-off at lower equivalence ratios than methane flames, lowering the lean blow-off limit from a range of 0.75 to 0.85 to values of 0.6 to 0.7. In addition, it was shown the former are less affected by the addition of CO_2 than the latter, allowing for burning at equivalence ratios under 0.6. Furthermore, emissions estimates for ideal flames showed a drop in NO_x levels for leaner conditions. A drop from a ϕ of 1 to 0.8 was estimated to drop NO_x emissions by roughly 80%, and emissions drop even further to about half for a base fuel with a 60/40% split of CH_4 and CO_2. Hydrogen addition in the fuel was shown not to significantly impact emissions.

Keywords: Low-Swirl Burner, Biogas, Hydrogen

1. Introduction

The current necessity for energy and power as a pillar for the development of world societies has led to an incessant increase in energy production demands, which for centuries has been largely met using fossil fuels. This practice has led to a number of environmental problems, among which the decrease of air quality due to the increase in air pollutants. Although combustion has been a staple of energy generation for centuries, this backdrop has urged a development of cleaner alternative methods. However, a need for combustion based power generation is still very much present, albeit with ever stricter restrictions, especially on emissions levels [1]. New power generation solutions have been developed, capable of not only reducing pollutant emissions but also allowing the possibility of using alternative, sustainable fuels.

The usage of biogas yields an even more optimistic outlook, as it can typically be sourced from Anaerobic Digestion (AD), a process which consists of the decomposition of biodegradable waste, a source which would not be utilized and possibly neglected [7]. Furthermore, it's often a by-product of agriculture and animal husbandry, meaning it would be comparatively inexpensive, especially if implemented in large scale. Despite these advantages, biogas is considered to be a poor fuel, largely due to the CO_2 within its composition [12, 9], and it often causes increased instability, oscillations and possibly blow-off, an adversity for low NO_x lean burning. Thus, biogas is a prime candidate for mixing with more reactive substances, such as Hydrogen H_2, notable for its high combustion rate, and in consequence its elevated flame speed, as well as its low lean combustion limits, properties which are desirable when burning Biogas. These differences in fuel properties comprise a fascinating challenge in adapting and attuning the available technologies to the contemporary requirements. The goal of this work is to investigate the effect of lean biogas combustion and hydrogen enrichment in small scale Low-Swirl burners, comparing flame geometry and stability limits for various compositions. Hence, 3 main goals can be defined:

1. The acquisition of non-reacting flow parame-

ters, and subsequent validation and quantification of the low-swirl flow field through Particle Image Velocimetry acquisitions;

2. The definition of stability limits for a number of fuel scenarios, and comparison of the effects of fuel compositions on them.

3. The estimation of the emissions in the ideal lean scenarios, and hypothesizing of the ultra low NOx claim for the LSB design.

2. Background

Low swirl burning (LSB) is an evolution of high swirl (HS) flames, relying on a similar flow geometry, but a different stabilization mechanism. While HS combustion relies on recirculation of the flow to anchor the flame, LSB relies on the propagating nature of premixed flames, stabilizing them through divergence of the flow. The LSB design has reliably allowed for the stabilization of lean flames at lower equivalence ratios and temperatures, reducing the emissions levels of pollutants, particularly the aforementioned NO_x, for which very low levels of under 5 ppm are possible under the leanest conditions, a significant improvement over the common high-swirl burner (HSB) design.

In any swirl burner, the initial challenge is to quantify a value to characterize the type and characteristics of the flow, and consequently of the flame. This dimensionless ratio is called the Swirl Number S_0 [5], and it represents a ratio between the axial fluxes of tangential and axial momenta, made non-dimensional by the burner radius, being represented as follows:

$$S_0 = \frac{G_\theta}{G_x R_b} \tag{1}$$

where G_θ is the axial flux of tangential momentum (kg m^2 s$_{-2}$), G_x refers to the axial flux of axial momentum (kg m s$_{-2}$), and R_b is the burner radius (m). A cylindrical coordinates system (x, r, θ) is considered for the axial, radial and tangential directions, respectively, with the dimensions in m, and the velocities (U, V, W) represent the velocities for each respective dimension (m s^{-1}). Should it be assumed that the flow is perfectly axisymmetric along the x axis, the fluxes of momentum are then defined by:

$$G_\theta = \int_0^{R_b} (Wr)\rho U 2\pi r dr \tag{2a}$$

$$G_x = \int_0^{R_b} 2\pi r \rho U^2 dr + \int_0^{R} 2\pi r p dr \tag{2b}$$

where ρ is the local density of the flow (kg m^{-3}) and p refers to the static pressure (Pa). The latter, however, is somewhat difficult to measure in an experimental apparatus as it requires various measurements of static pressure within the flow, possibly disrupting it. Thus, an alternative definition of the swirl number G'_x was established, substituting the contribution of the static pressure by an approximation using the tangential velocity [2], yielding:

$$G'_x = \int_0^{R_b} 2\pi r \rho \left(U^2 - \frac{1}{2} W^2 \right) dr \tag{3}$$

and resulting in a modified swirl number, hereby referred to as S, which, if constant density was to be assumed in the whole control volume, can be defined as:

$$S = \frac{G_\theta}{G'_x R_b} = \frac{\int_0^{R_b} r^2 U W dr}{R_b \int_0^{R_b} r \left(U^2 - \frac{1}{2} W^2 \right) dr} \tag{4}$$

This swirl number is fundamental to distinguish between low swirl and high swirl applications. A boundary was set at S equal to 0.6, above which the flow would be considered a high swirl flow, and below, a low swirl flow. The low swirl flows show relatively low flow divergence, and showed worse results for a typical HS layout.

2.1. Low Swirl Burners

Utilizing a burner of S in the region of 0.05-0.3, Chan et al. stabilized a detached low-swirl flame [2]. This design made use of the LSB properties and, due to deceleration of the flow, the flame would rest at a location where the flow velocity matched the local flame speed, creating a slight cup-like shape. Despite this, the flame showed properties resembling an ideal 1D combustion layout. The layout of this burner used air inlets from where air would be injected tangentially into the flow, generating swirl in the outermost zone of the burner flow. This method, however, required a dedicated burner design, negating the adaptability to smaller applications. To solve this issue, Yegian et al.[17] developed a novel solution to generate the desired flow conditions, creating a piece, called a swirler, which was divided into a central partial blockage of the flow aimed at causing a pressure loss, and consequent reduction of velocity, while still not generating recirculation, and an outer annular section composed of guide vanes which introduced the swirling motion onto the flow. This led to the development of a simplified swirl number calculation, based on the geometric parameters of this piece:

$$S = \frac{2}{3} \tan\alpha \frac{1 - (R_h/R_b)^3}{1 + (R_h/R_b)^2 \left((U_c/U_a)^2 - 1 \right)} \tag{5}$$

where α is the vane angle, R_h is the radius of the non-swirled centre hub (m), R_b is the burner outer

radius (m), with U_c referring to the bulk velocity for the central section $[0, R_h]$, and U_a to the bulk axial velocity in the swirled annulus $[R_h, R_b]$. Both flow bulk velocities are calculated by averaging the velocity in each respective section (m s^{-1}).

The swirler (and its associated S), is the fundamental piece of the current LSB design, as it is the piece responsible for generating the according flow field, and it's much cheaper, easier to produce and more adjustable than the previous implementation. An increase in S, either by increasing the angle of the vanes or decreasing the hub radius, will cause the flame to move upstream, and in extreme cases can cause significant recirculation and possible flame anchoring on the burner outlet, as the flame nears the high swirl condition. An increase in screen blockage yields a similar outcome, as it also increases the swirl number [16]. Extensive studies have been conducted on the fuel flexibility of the LSB setup, which have shown a broad acceptability range of fuels, particularly hydrocarbons [11]. This flexibility to the variation in fuel composition can be explained by the equilibrium equation for the velocity balance at the flame front [3]:

$$1 - \frac{dU}{dx}\frac{x_f - x_0}{U_\infty} = \frac{S_T}{U_\infty} = \frac{S_L}{U_\infty} + \frac{Ku'}{U_\infty} \qquad (6)$$

In this equation, U and U_∞ are the aforementioned axial velocity and bulk axial velocity, respectively, x_f represents the flame front coordinate in m, x_0 is a virtual origin of the flow, the point where velocity U is equal to the flow bulk velocity U_∞, also in m, K is an non-dimensional specific constant of the fuel, and u' is the root mean square (RMS) of the turbulent velocity fluctuations (m s^{-1}).

This equation, which applies for all self-similar LSB setups, approximates the divergence of the flow linearly, with a constant divergence ratio $a_x = (dU/dx)/U_\infty$ and represents the turbulent flame speed as a function of the turbulence intensity. This equation is applied on the centreline of the flow, where turbulence is mostly generated by the central screen of the swirler [10], and is proportional to the bulk velocity, which would mean the main factor for the flame brush position is S_L/U_∞. For most hydrocarbons, the laminar flame velocity does not vary significantly, and the flame brush position should not differ considerably, which holds especially true if the bulk velocity is significantly greater than the linear flame speed S_L. This poses problems for a fuel like hydrogen, for which the flame speed is significantly greater. Tests for the addition of H_2 to hydrocarbons showed the regular LSB stabilization mechanism remains unchanged until 60% H_2 [4], and the addition of hydrogen lowered the blow-off limit of the flames [11].

For the laboratory tests, the main goal was to verify the LSB's adaptability to varied compositions of biogas and the viability of its mixing with hydrogen. Both these fuels constitute attractive alternatives to the common fuels used for combustion, for different reasons. Biogas is a biofuel which is mainly composed of methane CH_4 and carbon dioxide CO_2, with other residual species. Although its origin is renewable, the wide variation of its composition poses challenges for the design of a burner system, as it has been shown that carbon dioxide has a considerable effect on the thermal inertia of the fuel due to its relatively high specific heat, which reduces flame stability and burning speed [12, 13].

Hydrogen, on the other hand, has very good combustion properties, and it has been proven to improve the lean stability of methane-air and syngas flames [11]. Its high burning rate and high mass heating value, combined with the absence of carbon molecules, make it an attractive fuel option, and it has been shown to increase efficiency in a variety of applications [15]. However, its increased flame speed can lead to flashback if the burner conditions are not ideal, and the increased flame temperature of hydrogen may lead to higher emission levels for comparable equivalence ratios.

3. Implementation

For the performance tests, a modular open flame LSB setup was assembled in the laboratory. Air flow was provided by a ventilator controlled by an AC power supply, attached to a Fluke 123 Series scopemeter. The ventilator was then linked to a settling chamber to stabilize the flow, and the burner was assembled on the end of this chamber. The swirler was placed upstream of the outlet, at a recess distance L_i of 1 inch, or $2R_b$. Also within this burner end were the fuel inlets, meaning the air/fuel mixture was formed at this point. Methane, hydrogen and carbon dioxide were bottle sourced, and the flow rates were controlled through a set of Alicat M-Series digital flow meters of varying capacities, ranging from 5 SLPM to 50 Standard Litres Per Minute.

The laboratory had available a pair of polymer swirlers from a previous installation using the same burner end, produced by injection moulding. These swirlers fit in the 25.4 mm (1 in) burner outlet diameter, and have 8 vanes at a fixed angle of 37^o. The ideal design for a swirler is considered to have vane angles of $30^o < \alpha < 42^o$ for hydrocarbons, and $30^o < \alpha < 35^o$ for high-hydrogen fuels to decrease the risk of flashback, and hence the swirler keeps a good compromise for the test fuels [16]. The centre section is 20 mm in diameter, and the screen that covers it is perforated with circular holes 1.5 mm in diameter, laid out in a square pattern, spaced at

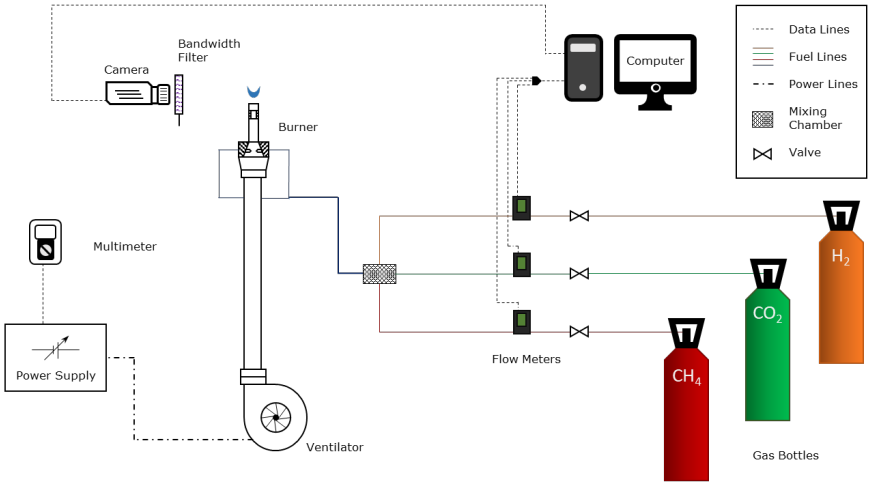

Figure 1: Setup for photo analysis.

regular 2.5 mm intervals. This results in a screen blockage of roughly 74% of the total area.

3.1. Camera/PIV Setup

Figure 1 depicts the layout for the camera setup assembled, as well as the burner setup and fuel sourcing system. A JAI CV-M9GE RGB camera was used for the flame photos attached to a Nikon AF Nikkor 50mm f/1.4D lens. The bandwidth filters were used with the aim of defining the location of the forming substances, and from there deducing flame shape. 3 types of filters were used, each restricting the incoming light to a substance's formation specific wavelength. The filters used had a bandpass centre wavelength of 516nm for the C_2 images, 431nm for the CH images and 451nm for the CO_2 images.

Particle Image Velocimetry (PIV) studies were undertaken as a non-intrusive way of defining the flowfield for this particular installation. The overall layout of the PIV setup is similar to the camera layout. However, while the camera layout was conceived for studies of a reacting flow, the PIV tests were undertaken using a non-reacting flow. This overrides the necessity for fuel supply, but adds the necessity for an air supply to provide the seeding particles for the PIV tests. Liquid paraffin was used to provide the seeding, and the flow meters were reused for the necessary air supply. One of the atomizers was then connected to the fuel inlet, while the other slowly released particles to fill the environment surrounding the burner outlet. This was made with the aim of defining the outer shear layer between the burner flow and the external environment. The laser used to illuminate the particles was of the Dantec DualPower 65-15 Nd:YAG type, synchronized to an ANDOR Zyla 5.5 sCMOS camera through a BNC Model 575 synchronizer. The camera made use of a Nikon AF Nikkor 60mm f/1.28D lens, set to its largest aperture (f/1.28), coupled to a Meller Griot bandwidth filter of 532nm wavelength. All results were obtained and processed using the Dantec DynamicStudio 5.1 software.

3.2. Image Processing

For each fuel condition, a set of 5 images was obtained to allow the calculation of a more representative average for the flame at each set point. All cases had visibility issues for leaner flames, which would cause the software to struggle with defining flame boundaries. Therefore, each type of photo was processed independently to make sure the flame was visible under all conditions, while still keeping the pictures of the richer flames from saturating. The flames were processed in brightness and converted to a binary scale to define the boundaries. The PIV images were acquired in sets of 400 pairs of images at a frequency of 15 Hz, with a time between pulses of 20 ms. The velocity calculations were made using cross correlation, by dividing the image into Interrogation Areas (IA) of 32x32 px in size, with an overlap of 25% in both directions. The 400 results were then filtered and averaged to provide the flow field for each case.

3.3. Fuel Test Conditions

For the reacting flows, fuel conditions were set so that the molar fractions of the species in the fuel were constant, so that a good comparison on the impact of the variation of each component could be obtained, and the power of the flame was kept constant. The calculation of the flame power was made using the following equations:

$$P = \dot{m}_f \overline{LHV} = \dot{n}_f LHV = \frac{p\dot{V}_f LHV}{R_0 T} \qquad (7)$$

A set of 12 conditions were set. To simulate biogas, two mixtures of CH_4 and CO_2 were considered, one with 80% methane and 20% carbon dioxide, and another with 60% CH_4 and 40% CO_2, in addition to a pure methane condition. Subsequently, 4 percentages of H_2 were mixed into the overall flow (0, 10, 20 and 30%). As the temperature and pressure conditions were considered to be uniform for all the species, the volume flows for each set condition, as set by the flow meters, must follow these restrictions. Thus, the stoichiometry ratio for any biogas and hydrogen combination was given by:

$$\phi = \frac{(2y_{CH_4} + 0.5y_{H_2}) * 4.76}{\left(\frac{\dot{V}_{air}}{\dot{V}_f}\right)} \tag{8}$$

where $\dot{V}_f = \dot{V}_{CH_4} + \dot{V}_{H_2} + \dot{V}_{CO_2}$. Power of the flame was calculated through the lower heating value of the fuel, using Equation 7. A base power value of $P = 5.88$ kW was set to be used by all flames. For combinations, the power equation was defined as:

$$P\frac{R_0 T}{p} = \dot{V}_{H_2} LHV_{H_2} + \dot{V}_{CH_4} LHV_{CH_4} \tag{9}$$

3.4. Air Flow Calculations

To obtain the air flow through the burner outlet, a numerical integration process was defined to integrate the velocity profile along the outlet surface. The integral which yields the flow rate, considering an axisymmetric velocity profile, is defined as:

$$\dot{V}_{air} = \int_0^{2\pi} \int_0^{R_b} V r dr d\theta \tag{10}$$

Since the function for the velocity at the burner outlet is discrete, a trapezoidal numerical integration was used to calculate the flow rate. In the radial integration a factor of r has to be multiplied by the velocity function, meaning, for the numerical integration a secondary function $g(r) = V(r) * r$ was defined and numerically integrated between 0 and R_b. To take into account the asymmetry of the velocity profile, a second integration was made between $-R_b$ and 0, which was then averaged with the positive integration and multiplied by 2π to obtain the results.

3.5. Emission Calculations

To estimate the emissions for an LSB flame, adiabatic 1D flames were made using Cantera, an open-source Python module, to simulate the propagating LSB flame. The simulations were conducted using the GRI Mech 3.0 mechanism, which calculates a 1D adiabatic flame at a pressure of 1 atm and burner temperature of 300 K by defining the reaction rates for 53 species, totalling 325 reactions. The simulation is considered to provide the final combustion products fraction when the adiabatic temperature is reached. For this study, the simulation was run for equivalence ratios of $0.8 < \phi < 1.2$, delivering results for NO_x for the set conditions, which were considered to be the sum of NO and NO_2, as well as adiabatic temperature, which is related to the formation of these species.

4. Results

4.1. PIV Flowfields

Non-reacting PIV studies were made to define the flow field at the burner's outlet, specifically, in both a perpendicular plane and a parallel plane to the burner outlet at the minimum distance achievable. This distance was estimated to be less than 2 mm, and the plane was effectively defined as the $x = 0$ plane.

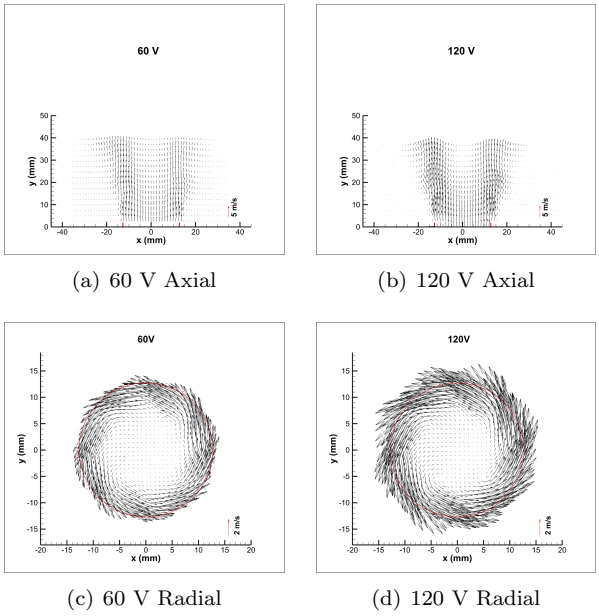

(a) 60 V Axial (b) 120 V Axial

(c) 60 V Radial (d) 120 V Radial

Figure 2: Axial and tangential velocity maps.

Tests with the pre-seeded environment were made, showing results in line with the expected results for an unconfined flow at the tested Re [8] for a LSB layout. Further tests were then made for 10 different ventilator voltage levels: 20, 30, 40, 60, 80, 100, 110, 120, 130 and 140 V. Figure 2 shows results for two voltages (60 V and 120 V), from which the similarities of the two flows can be assessed.

Flow field analyses show a well defined Low Swirl environment both in the horizontal and vertical planes, and in both cases the lower velocity axial flow centre section and the higher velocity annular swirled flow section are distinguishable, providing cup-shaped streaklines on the (r, x) plane, on which a flame can stabilize, forming the typical cup-shaped LSB flames. The results in the (r, x) plane also showed the divergence of the flow, exhibiting

a noticeable radial component to the velocity, particularly in the outermost part of the swirled annulus. This causes the flow to expand in the radial direction into the environment and slightly increase the size of inner annulus x, sharply reducing axial velocity of the overall flow. This is one of the staples of the low swirl burner's adaptability, as the divergence of the flow allows the flame to stabilize at the location where the flow velocity is equal to the turbulent burning velocity S_T, regardless of the conditions which affect it (such as ϕ or the fuel properties). Results also show, particularly for the higher velocity (120 V), a very low velocity area in the centre of the flow, showing that this particular flow field is at a swirl number on the upper scale of low swirl, almost generating a recirculation bubble. Other measured flow fields showed results consistent with these. The velocity profiles at the burner exit also show similar results. A clear distinction between the non-swirled centre and the tangentially swirled annulus can be recognized, more clearly in the tangential flow profile than in the axial one.

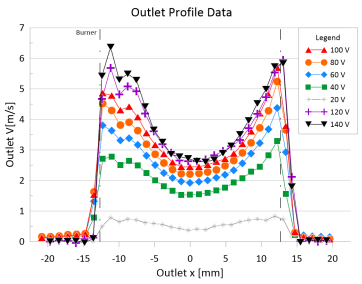

(a) Axial Profiles

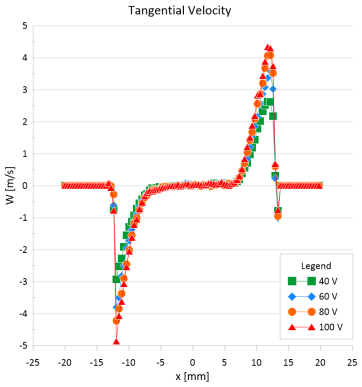

(b) Radial Profiles

Figure 3: Axial velocity and tangential velocity profiles at the burner exit centreline.

Moreover, both the flow field map results and the profile results show that the flow characteristics remain largely the same for all ventilator voltages, with the velocity vectors changing largely only in scale, except for the 20V case, as this low voltage yields a relatively small fan speed, leading to very small bulk velocity and a flow resembling a plug type flow rather than a typical swirling flow. This particular result was therefore discarded from any calculations relating to the swirling flow, especially seeing as flow velocities this low weren't used in any of the flame tests. However, the flow rate was taken into account,as the axial flow rate is independent from the flow geometry.

Having obtained the profiles of the velocity in both planes permitted the calculation of S using either of the previously defined equations. The fluxes of momentum were numerically calculated, and the swirl numbers were obtained for the nine measured voltage settings. Results showed the swirl number to be roughly constant around a value of 0.5, which is typical for LSB setups [16].

4.2. Ventilator Calibration

With the velocity profiles defined, the calculation of the axial flow rate can be made by simply integrating, in cylindrical coordinates, the axial velocities within the burner diameter as discussed in section 3.4. From this flow rate an average bulk velocity can be determined, and the Reynolds number can be calculated.

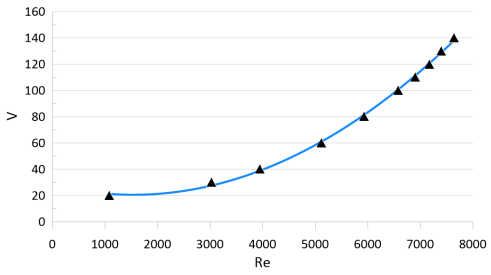

Figure 4: Inverse of Re in function of voltage, and respective fit curve.

Figure 4 shows the points corresponding to the calculated Re for each voltage setting, showing a quadratic correlation between the voltage and Re (and thus the flow rate). From this result, and with the aim of obtaining a better fit, the variables were switched to obtain an equation for voltage as a function of Re. The curve fit found was $V_{vent} = 3e-6 * Re^2 - 0.0097 * Re + 28.03$, with a coefficient of determination of $R^2 = 0.99885$, and that equation was numerically solved in order to obtain Re as a function of the voltage.

4.3. Flame Characterization

Flame photos were obtained for the fuel conditions previously described, for equivalence ratios of $\phi = 0.9$, $\phi = 1$ and $\phi = 1.2$. In addition to that, pictures using 3 types of bandwidth filter were taken for a total of 140 pictures. As both the power and the fuel composition were firmly defined, the air flow rate was adjusted by adjusting the ventilator voltage. However, the Reynolds numbers for

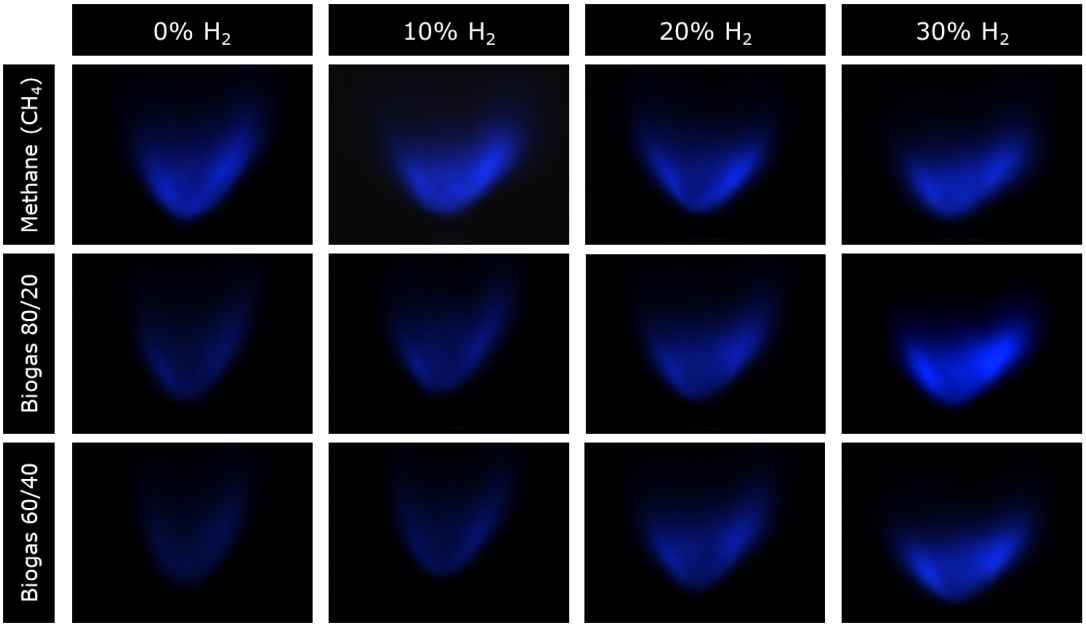

Figure 5: Unfiltered flames for $\phi = 1$. Top Row: Methane; Middle Row: 80/20 Biogas; Bottom Row: 60/40 Biogas. Left to Right: 0, 10, 20, 30% H_2.

all tests did not differ widely, and were well within the same order of magnitude, which, in conjunction with the PIV results assures similarity of the flow across all conditions.

Flames at a stoichiometric equivalence ratio with no filter are represented in Figure 5, and they show the effects of fuel composition on the flame size, shape, position and brightness. For a particular composition of fuel, a number of parameters can influence any, or all in fact, of these characteristics. As a method of analysis, the first impact studied will be that of the variation of hydrogen in the fuel. As mentioned, hydrogen is an extremely volatile fuel, particular for its faster combustion chemistry, and consequent high flame speed. Flame shape, size and position can all be examined in a more intuitive manner by way of the brightness contours created for each composition of flame. As the most representative example of flame shape change for these conditions, the outlines of the four hydrogen percentages for a 60/40 mixture of biogas were chosen, and are represented in Figure 6.

From the outlines, 3 conclusions are easily drawn. The first is that an increase in hydrogen fraction largely corresponds to a much more easily visible flame. This is associated with the higher brightness levels for greater hydrogen fractions, largely in part due to its fast combustion rate. The second is that an increase from 0% H_2 to 10% anchors the flame slightly downstream, a result which is counter-intuitive with the tendency for hydrogen addition. However, if the hydrogen percentage was to be further increased, the flame would move upstream and settle at a position where the flow velocity is higher, a result of the effect of its higher flame speed on the fuel. Another significant effect noted was the widening of the flame as the H_2 percentage rose. Hydrogen flames tend to be shorter than those of hydrocarbons, which leads the flame to propagate in the axial direction. This results in wider, yet flatter flames and can, together with the increased flame speed, cause the flame to anchor at the burner outlet.

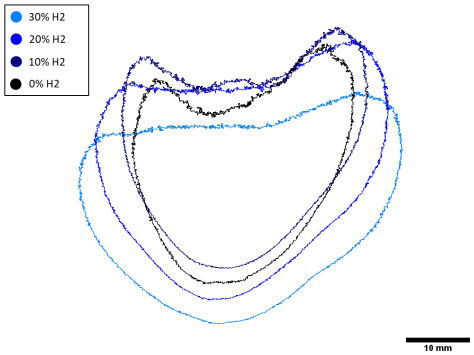

Figure 6: Flame outlines for 60/40 Biogas flames at $\phi = 1$.

Effects of CO_2 are also observable by comparing the flames in the columns of the grid. An increase in carbon dioxide fraction has the reverse effects of hydrogen addition: the inert nature of CO_2 draws energy from the flame, reducing its brightness [14]. Furthermore, the slower combustion chemistry of biogas leads the flame downstream and into a more

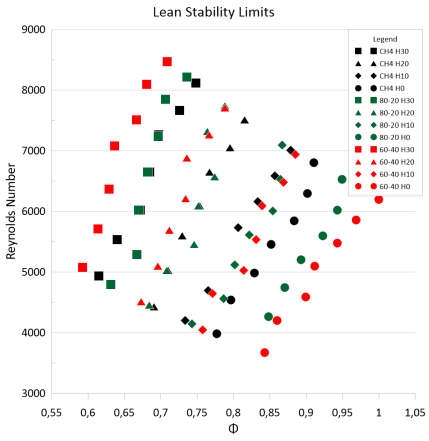

Figure 7: Blow-off limits for the test fuel compositions.

closed and elongated, tulip-like shape, as opposed to the wider, shorter bowl-like shape of high CO_2 percentage flames.

4.4. Stability

Previous studies have shown the effects of biogas composition and hydrogen in other types of flames, and the general consensus shows higher levels of CO_2 in the biogas composition tend to worsen flame stability by increasing the lean flame limit, causing the flame to quench at higher ϕ. This is due to the addition of an inert component with a relatively high heat capacity, while the addition of hydrogen tends to improve flame stability by lowering the lean flame limit, due to both the higher LHV and higher combustion rate. [9, 18] To assess the effect of biogas composition, as well as hydrogen addition, lean stability tests were conducted for the fuel conditions. The flashback limits were not measured in this case as the LSB is designed for better performance while burning a lean premixed flame. The fuel flows were set, and the ventilator was gradually adjusted to a higher velocity setting, until the flame was extinguished. This process was repeated at least 3 more times for each case until an agreeable value was reached.

Figure 7 shows the results obtained from the stability tests. As expected, the blow-off limits unanimously and monotonically rise with the increase in Re, showing the highest amplitude of results of ϕ in the region of 0.15 for the 60/40 biogas mix with no hydrogen. On the other hand, flames based on pure methane, with no addition of CO_2 tend to show less variation of blow-off limits, and for certain cases, such as the pure methane flames, show an inflexion towards keeping the blow off equivalent ratio constant for higher Re.

The addition of hydrogen also showed the expected effect in the flame stability. Previous tests, both with LSB setups [11] and other types of burners [18] show that the addition of hydrogen significantly reduces the flame stretch rate, thereby avoiding local quenching of the flame and significantly lowering the blow-off limits of the methane/biogas flames. A particularly interesting result is revealed when the addition of CO_2 is considered and compared to other flames with the same molar fraction of hydrogen. Flames with no hydrogen show a decrease in flame stability, significantly raising the blow-off limit, and for these conditions the addition of 40% CO_2 results in an increase of the blow-of ϕ of roughly 0.1, on average when compared to the methane flames. However, as hydrogen is added, that difference is reduced and for flames with 20% H_2 or over the biogas flames show lower blow-off limits when compared with the mixture of methane and hydrogen. Although this situation benefits from the highest value of both H_2 flow rate and total flow rate, it nonetheless shows a trend for a larger relative influence of hydrogen on biogas flames.

Another property of the LSB which was verified during testing was its sturdiness under transient conditions. As a general rule, when the fuel composition was changed, the flame simply adjusted to the position which matched the local flame speed, without the need to relight the burner. This shows the robustness and flexibility of the LSB design for a variety of fuels, and means the burner should be able to hold fluctuating fuel compositions, provided these are within the stability boundaries.

4.5. Emissions

As described in Subsection 3.5, simulations for a one dimensional adiabatic flame were made. Although the LSB flames are not perfectly planar nor adiabatic, the propagating nature of the LSB design means its flame has been shown to be relatively similar to the 1D approximation used in the simulations. Thus, the results are still relevant for the LSB combustion, as they can show trends for the changes in the parameters of interest in this study, namely, biogas composition, hydrogen addition and equivalence ratio.

Figure 8 shows the molar fraction of NO_x in the combustion products (in ppm) and the adiabatic temperature comparison for methane and the two biogas compositions, and their respective mixing with 10, 20 and 30% H_2. NO_x is largely formed by way of one of three main mechanisms [6]: thermal (or Zeldovich), prompt (or Fenimore), and fuel. Thermal NO_x refers to the oxides that are generated under relatively large temperatures (usually over 1600 °C), and is the mechanism by which most os the NO_x is generated under conditions close to stoichiometry. Prompt NO_x was proposed by Fenimore, and describes the mechanism by which car-

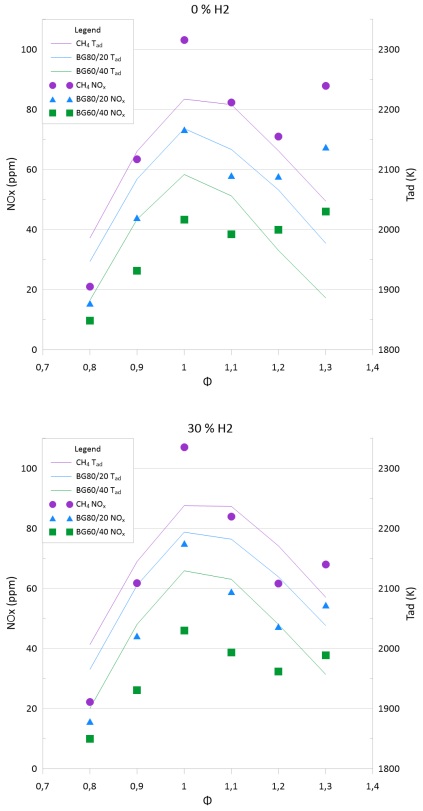

Figure 8: NO_x emission levels (in ppm) and adiabatic flame temperature (K) for 0 and 30% H_2.

bon based fuels under rich conditions react with the nitrogen molecules, and this mechanism is much more significant under rich conditions. Fuel generated NO_x is relevant for fuels with a significant nitrogen fraction, which is not the case. Therefore, for this case, NO_x formation is ruled by the thermal and prompt mechanisms.

Results show a typical adiabatic temperature distribution as a function of ϕ, showing a peak around $\phi = 1$. Although the addition of a higher hydrogen component does not seem to affect the adiabatic temperature of the flame much, which is expected as the adiabatic temperature of H_2 is only marginally superior to that of CH_4, the addition of CO_2 to the fuel reduces the adiabatic temperature, due to the aforementioned heat capacity of carbon dioxide. As mentioned, the main mechanism for NO_x generation under lean and stoichiometric conditions is thermal, and pollutant levels share the same trend as the adiabatic temperature, and follow the slight increase for the fuels with a greater fraction of hydrogen. However, for the rich conditions, the dominating mechanism becomes the prompt NO_x formation, which explains the slight drop as temperature drops after stoichiometry, and the subsequent rise as ϕ rises.

For low NO_x LSB operation, lean conditions are always desired, as the effect of the prompt mechanism becomes minimal, and the effect of the thermal mechanism is heavily reduced. Adiabatic results show low levels of NO_x of about 20 ppm, or less for the biogas based fuels, showing a sharp reduction under the leaner conditions. Results showed that neither the addition of hydrogen nor biogas increased the emissions levels considerably, with the addition of biogas reducing the NO_x emissions. If these results are taken into account with the stability results, showing a possibility of stabilizing flames for equivalence ratios as low as 0.5 by adding hydrogen, a very good case can be made for the very low NO_x claim of previous studies for the LSB.

5. Conclusions

This work was divided into three main objectives. The first one was to confirm the feasibility of an LSB burner, 2.54 cm in diameter, in the laboratory. For this, PIV images were obtained for a range (20 V to 140 V) of ventilator velocities. From these, the typical LSB flow field was observed, both in a plane normal to the burner exit and a plane parallel to it, and S was found to be within the low-swirl operating interval.

The second objective was to evaluate the effects of using biogas as a fuel, and enriching it with hydrogen. A set of conditions was established, and the effect of the addition of each species was then analysed in two different ways. Firstly, the flame properties were assessed by observation of the flame images, which were then processed to obtain a brightness based outline of the flame, helping evaluate parameters such as flame shape and position. Results showed that the increase of the fraction of carbon dioxide in the biogas mixture causes the flame to become dimmer, to anchor in a position further downstream and to have a more elongated shape. The addition of hydrogen had the opposite effect on the flames, causing generally shorter, wider more upstream and more intense flames than the ones with no hydrogen content. These effects of hydrogen addition were more noticeable in the flames with higher levels of CO_2. The LSB was also able to hold the flame in the transient conditions between the set points. Flame limits were then studied to evaluate the adaptability of the LSB design to the fuel conditions. Again, it was observed that the addition of CO_2 was detrimental to the flame properties, and it caused the lean limit of methane flames to rise significantly. However, hydrogen was proved to substantially improve the lean stability of the flames, especially for fuels with more CO_2, partly dissimulating the negative effects of carbon dioxide.

Lastly, simulations were made for the same conditions, with the goal of obtaining a trend for the effects of fuel composition on the emissions of NO_x.

The overall trend of results for ϕ was consistent with the expected results considering the NO_x formation mechanisms. Higher fractions of carbon dioxide were shown to reduce NO_x levels, while hydrogen addition was shown not to have a significant impact on NO_x formation. These results also set a very positive tendency for very low NO_x levels in leaner regimes ($\phi < 0.8$), validating the LSB design as a low-NO_x technology.

References

[1] E. E. Agency. European union emission inventory report, 2017.

[2] C. K. Chan, K. S. Lau, W. K. Chin, and R. K. Cheng. Freely propagating open premixed turbulent flames stabilized by swirl. *Symposium (International) on Combustion*, 24(1):511–518, 1992.

[3] R. K. Cheng, D. Littlejohn, W. A. Nazeer, and K. O. Smith. Laboratory studies of the flow field characteristics of low-swirl injectors for adaptation to fuel-flexible turbines. *Journal of Engineering for Gas Turbines and Power*, 130:021501 1–10, 2008.

[4] R. K. Cheng, D. Littlejohn, P. A. Strakey, and T. Sidwell. Laboratory investigations of a low-swirl injector with h_2 and ch_4 at gas turbine conditions. *Proc. of the Combustion Institute*, 32:3001–3009, 2009.

[5] N. A. Chigier and J. M. Beér. Velocity and static-pressure distributions in swirling air jets issuing from annular and divergent nozzles. *Journal of Basic Engineering*, 23:788–796, 1964.

[6] M. C. Drake and R. J. Blint. Calculations of nox formation pathways in propagating laminar, high pressure premixed ch4/air flames. *Combustion Science and Technology*, 75:261–285, 1991.

[7] G. Esposito, L. Frunzo, A. Giordano, F. Liotta, A. Panico, and F. Pirozzi. Anaerobic co-digestion of organic wastes. *Reviews in Environmentsl Science and Bio/Technology*, 11:325–341, 2012.

[8] A. Frank, P. Therkelsen, M. S. Aznar, V. H. Rapp, R. K. Cheng, and J. Y. Chen. Investigation of the down-scaling effects on the low swirl burner and its application to microturbines. *Proc. of ASME Turbo Expo 2018: Turbomachinery Technical Conference and Exposition*, GT2018–77208, 2018.

[9] Z. Hu and X. Zhang. Experimental study on flame stability of biogas/hydrogen combustion. *International Journal of Hydrogen Energy*, 44:5607–5614, 2019.

[10] D. Littlejohn and R. K. Cheng. Fuel effects on a low-swirl injector for lean premixed gas turbines. *Proc. of the Combustion Institute*, 31:3155–3162, 2007.

[11] D. Littlejohn, R. K. Cheng, D. R. Noble, and T. Lieuwen. Laboratory investigations of low-swirl injectors operating with syngases. *Journal of Engineering for Gas Turbines and Power*, 132:011502 1–8, 2010.

[12] L. Pizzuti, C. A. Martins, and P. T. Lacava. Laminar burning velocity and flammability limits in biogas: A literature review. *Renewable and sustainable Energy Reviews*, 62:856–865, 2016.

[13] F. Quintino and E. Fernandes. Analytical correlation to model diluent concentration repercussions on the burning velocity of biogas lean flames: Effect of co2 and n2. *Biomass and bioenergy*, 119:354–363, 2018.

[14] F. Quintino, T. P. Trindade, and E. Fernandes. Biogas combustion: Chemiluminescence fingerprint. *Fuel*, 231:328–340, 2018.

[15] C. D. Rakopoulos and C. N. Michos. Generation of combustion irreversibilities in a spark ignition engine under biogas–hydrogen mixtures fueling. *International Journal of Hydrogen Energy*, 34:4422–4437, 2009.

[16] P. Therkelsen, D. Littlejohn, and R. K. Cheng. Parametric study of low-swirl injector geometry on its operability. *Proc. of ASME Turbo Expo 2012*, pages 309–318, 2012.

[17] D. T. Yegian and R. K. Cheng. Development of a vane-swirler for use in a low no_x weak-swirl burner.

[18] H. Zhen, C. W. Leung, C. Cheung, and Z. H. Huang. Combustion characteristic and heating performance of stoichiometric biogas-hydrogen-air flame. *International Journal of Heat and Mass Transfer*, 92:807–814, 2016.